Accepted for publication in *The Journal of Geophysical Research,* Oct. 12, 2000

Observations of the seasonal dependence of the thermal plasma density in the southern hemisphere auroral zone and polar cap at 1 Re

M. T. Johnson, J. R. Wygant, C. Cattell

School of Physics and Astronomy, University of Minnesota, Minneapolis, MN

F. S. Mozer and M. Temerin

Space Science Laboratory, University of California, Berkeley, CA

J. Scudder

Department of Physics and Astronomy, University of Iowa, Iowa City, IA

Abstract. Synoptic maps of the thermal plasma density in the auroral zone and polar cap around 1 Re altitude are produced from measurements of Polar spacecraft floating potential during 1 year of perigee passes. The densities are accurate to around a factor of 2 in this region of space. These measurements, which provide the first comprehensive maps of the thermal plasma density over the polar cap and auroral oval, show clear variations in plasma density due to solar illumination of the ionosphere. Number density increases by a factor of 5 for illuminated verses non-illuminated ionospheric conditions over the entire auroral oval and polar cap. The maps delineate the global extent of the large scale auroral density cavity near 70 $\pm$ 5 degrees invariant latitude. These maps further show that the depth of the density cavity is strongly influenced by solar illumination. The minimum average density ($\sim$0.1 cm^{-3}) occurs in darkness near 19 MLT.

1. Introduction

The existence of a large scale density depletion on auroral magnetic field lines was first demonstrated by *Mozer et al.* [1979, 1980] using Langmuir probe data from the S3-3 satellite. *Calvert* [1981], using measurement of the upper hybrid line as the density diagnostic, showed that a density cavity with a spatial extent of about 6 degrees invariant latitude existed over an altitude range of 1 - 3 Re on auroral field lines. *Persoon et al.* [1988] provided a map of the auroral density cavity in the afternoon to midnight local time sector using densities determined from the plasma frequency cut off of the whistler mode auroral hiss observed by the DE-1 spacecraft. This work demonstrated that the cavity was strongest on the night-side and that the densities could fall as low as 0.1 cm^{-3}. Other local time sectors were not explored due to the lack of orbital coverage by the DE-1 wave instrument. In addition, these studies could not determine density variations throughout the entire latitudinal extent of the cavity because auroral hiss is typically only present at its pole-ward edge. The study presented here extends the local time coverage to the day-side and the early morning local time sector and covers all latitudes in the polar cap and auroral zone. The spatial and seasonal variations in plasma density present throughout the polar cap and auroral zone may also be observed because of the extensive coverage of the Polar data set.

The thermal plasma structure near 1 Re altitude on auroral magnetic field lines is of particular interest because experimental evidence from S3-3 [*Mozer et al.*, 1977; *Temerin*, 1984], Viking [*Boström et al.*, 1988;

Block and Fälthammar, 1991], and now Polar [*Mozer et al.*, 1997] and FAST [*Ergun et al.*, 1998; *Carlson et al.*, 1998] indicates that intense, non-linear electric field structures exist at this altitude. These electric fields can accelerate electron beams downward, generating aurora, and accelerate ion beams away from the earth. Intense waves in this region are responsible for the generation of ion conics which are also accelerated away from the earth [*Shelley*, 1995]. The plasma density structure is important in these processes because it affects the propagation and generation of waves and the availability of current carrying particles. Thus, there is the possibility of a variety of non-linear mechanisms involving feedback between the electric fields that accelerate the charged particles, the creation of density depletions, and the modification of the electric fields as they interact with the density cavity.

2. Data Analysis

The measurement of number density in rarefied plasmas is a difficult task, and several complementary methods have been used to provide information on the structure of the thermal plasma in the terrestrial magnetosphere. The spacecraft potential, measured using the Polar Electric Field Instrument (EFI) [*Harvey et al.*, 1995], is used as a plasma density diagnostic for this study. The Polar EFI measures the spacecraft potential by finding the potential difference, ΔV, between the surface of the spacecraft and an electric field probe biased to float near the local plasma potential. This technique can provide almost routine, continuous information about the thermal plasma density. Coverage of the Polar data set allows seasonal variations of the entire auroral oval and polar cap to be observed over several years. Reviews of the technique, comparison to other techniques, scientific results, and references may be found in *Pedersen* [1995], *Escoubet et al.* [1997], *Laakso et al.* [1997], and *Laakso et al.* [2000].

Theoretically, the spacecraft potential is determined primarily by the balance between the thermal current to and the electron photo-current from the spacecraft surface. The spacecraft potential is, in general, affected by electron temperature and density variations of the electron thermal current. However, it has been shown [*Pedersen*, 1995] that the floating potential of the spacecraft is an indicator of electron plasma density for Debye lengths much larger than the spacecraft radius. This is caused by the "focusing effect" which is due to low energy electrons drawn to the spacecraft reducing the effect of electron temperature on the spacecraft potential. Previous studies calculated the spacecraft floating potential assuming an infinite Debye length. Plasmas in the polar cap and auroral oval at 1 Re with typical densities (0.1 to 100.0 cm^{-3}) and temperatures (1.0 to 5.0 eV) [*Kletzing et al.*, 1998] have Debye lengths ranging from about 0.7 to 50 m which is on the order of the spacecraft dimensions. Therefore, the assumption of infinite Debye length is not appropriate. In order to assess the accuracy of the spacecraft potential as a density indicator in these regions, we use the more general expression [*Mott-Smith and Langmuir*, 1926; *Schott*, 1995] to represent the flux of thermal electrons on the spacecraft. We assume a Maxwellian plasma distribution. The satellite body is approximated by a spherical conductor because the spacecraft diameter and height are on the same order of magnitude (d=2.4 m, h = 1.8 m). This is a better approximation of the spacecraft size than the cylindrical case where it is required that $h >> r$. The thermal current density is then

$$j_e = \frac{4\pi s^2}{4\pi r^2} I \left(1 - \frac{s^2 - r^2}{s^2} e^{-r^2\eta/(s^2-r^2)}\right) \qquad (1)$$

Here $\eta = eV/T$ is the ratio of the spacecraft floating potential to the the electron temperature, r is spacecraft radius, and I is the thermal current density for an uncharged spacecraft. The sheath length, s, is estimated by the radius of the spacecraft plus the Debye length.

$$s = r + 7.43\sqrt{\frac{T}{n}} \qquad (2)$$

Here T is the electron temperature in eV and n is the electron density given in cm^{-3} with the Debye length given in meters. This expression effectively limits the focusing effect by excluding particles with impact parameters more than a Debye length away from the spacecraft surface.

Several studies have addressed the issue of the photoemission current density from a satellite body [*Grard*, 1973; *Pedersen*, 1995; *Nakagawa et al.*, 2000]. In particular, *Scudder et al.* [2000] have derived the photoemission current density as a function of spacecraft potential for the Polar spacecraft by performing a detailed statistical analysis using nearly 10 months, from May 1996 to June 1997, of the spacecraft potential from the Polar EFI and plasma measurements from the Polar Hydra instrument [*Scudder et al.*, 1995].

$$j_\nu = ae^{-eV/b} + ce^{-eV/d} \qquad (3)$$

Here a=152μAm^{-2}, b=1.65 eV, c=0.86μAm^{-2}, d=9.49 eV are constants. The total electron current to and from

the spacecraft can be found by multiplying the thermal current and photo-current densities by the total spacecraft area, A, and illuminated area, A_ν, respectively. Figure 1 shows the total photo-current from, $j_\nu A_\nu$, and the total thermal current to, Aj_e, the satellite body as a function of spacecraft potential for varying electron temperatures. Values used for the areas are $A = 22.6m^{-2}$, $A_\nu = 6.16m^{-2}$, with $A/A_\nu = 3.67$. The upper panel assumes an infinite Debye length plasma. The lower panel assumes a finite Debye length plasma using equation (2) to estimate the sheath length for varying plasma densities and temperatures. The equilibrium condition is when these two currents are equal,

$$A_\nu j_\nu = A j_e \tag{4}$$

The thermal density can be solved for as a function of the spacecraft potential, V, for various fixed temperatures and compared to experimental results produced by *Scudder et al.* [2000].

$$n = ae^{-eV/b} + ce^{-eV/d} \tag{5}$$

where a = 1.2e4 cm^{-3}, b = 0.81 eV, c = 6.89 cm^{-3}, and d = 4.52 eV. Equation (5) presents an electron density curve produced from an analysis of Hydra electron data from May 29, 1996 for which $A/A_\nu = 3.67$. The density values at very low potentials were derived from UHR points provided by the Plasma Wave Instrument. Figure 2 presents the solution to equation (4) for plasma temperatures from 1 to 5 eV compared to equation (5). The calculated result is within around a factor of two from the experimental curve for densities between 0.1 to 100 cm^{-3} with temperatures between 1.0 and 5 eV. Therefore, the experimental calibration, Equation (5), should be good to about a factor of two for densities from 0.1 to 100.0 cm^{-3} in the polar cap and auroral oval. These results are in good agreement with those by *Pedersen* [1995] and *Escoubet et al.* [1997] using GEOS-1, GEOS-2 and ISEE-1 measurements.

Scudder et al. [2000] have pointed out that this curve varies seasonally due to changes in the area of the spacecraft illuminated by the sun as the orbital plane of the spacecraft precesses through the year. The change in illuminated area is less than 10% of the total area and reaches a minimum in the noon-midnight meridian. Spacecraft illumination effects would appear as an overall increase in density along the noon-midnight meridian. This effect is not visible in the plots of electron density shown here.

The data used to create the synoptic maps are obtained from the Polar key parameter files from over 420 perigee passes covering the period from April 15, 1996 to April 15, 1997. The data are converted to plasma number density using equation (5) and then thirty second averages are binned in magnetic local time and invariant latitude and averaged. Because the measured value of the spacecraft potential, ΔV, is relative to a EFI probe biased to float ~2V above the local plasma potential, the floating potential of the satellite relative to the plasma is $V = \Delta V + 2V$. This offset must be added before measurements are converted to number density [*Scudder et al.*, 2000]. Times when the spacecraft is in shadow, for which $V < 0V$, and when the Plasma Source Instrument (PSI) is active, causing the spacecraft potential to be fixed at 2V, have been removed from the data set.

3. Results

To show the average number density variation due to seasonal and ionospheric illumination, synoptic maps of the entire southern hemisphere have been made. Data are plotted vs. invariant latitude and magnetic local time. The color scale saturates at 100 particles cm^{-3}. Regions where there is an absence of data on a given map are white.

Plates 1a and 1c show data from April 15, 1996 to October 15, 1996 (southern hemisphere "winter") and October 15, 1996 to April 15, 1997 (southern hemisphere "summer") respectively. The map during the winter months (Plate 1a) shows a clear, large scale plasma depletion in the pre-midnight sector of the auroral zone at 70 ± 5 degrees invariant latitude. Other regions of low density are seen in the pre-dawn sector from 2 - 6 MLT and in the post-noon sector from 15 - 18 MLT. The average magnitude of the density in the cavity is less than 5 cm^{-3} with minimum average densities less than 1 cm^{-3} around 20 MLT. Individual line plots before averaging (Figure 3, for example) indicate that lowest densities of about 0.1 cm^{-3} are observed near dusk. The density for invariant latitudes less than 65 degrees and in the polar cap ranges from 20 to 100 cm^{-3}. There is a clear enhancement of the plasma density by a factor of 5 over the entire polar cap and auroral zone during the summer (Plate 1c). Effects of individual orbits, such as the line shaped enhancement on the dawn side of the polar cap (Plate 1a), are visible.

To determine whether the seasonal effects seen in Plates 1a and 1c are due to variations in ionospheric illumination, the data have been sorted by whether the measurement was made when the foot-point of the field line was in sunlight or in darkness. The resulting maps

are shown in Plates 1b (non-illuminated) and 1d (illuminated). The same general features which were observable in the seasonal maps can still be seen. There is a density cavity at the average location of the auroral oval both under sunlit and dark conditions, with the average density under darkness being approximately a factor of 5 less than in sunlight. The primary difference between Plates 1a and 1b is that Plate 1b shows that, in darkness, the deep density cavity extends to the day-side except from $\sim$ 11 to 12 MLT. In addition, the average density in the day-side polar cap is also lower than in 1a. These effects indicate that the density variations seen in the seasonal maps are due to solar illumination.

In in order to provide an indication of the small scale fluctuations of the electron number density such as those shown in Figure 3, the standard deviation normalized by the average is displayed in Plate 2 and the minimum values in each bin are displayed in Plate 3. The standard deviation is higher from around 19 MLT in the pre-midnight sector to 2 MLT in the post-midnight sector between 68 to 75 degrees invariant latitude under winter or non-illuminated (Plates 2a and 2b) conditions. This location corresponds to the location of the plasma density cavity shown in Plate 1. The increase in the standard deviation is not present in the summer (illuminated) case. The variation in the polar cap is slightly lower for summer conditions compared to winter. The increase in standard deviation in the post-midnight summer case and the portion of the polar cap on the sun-ward side of the dawn-dusk meridian during winter is mainly due to the mixing of data from illuminated and non-illuminated foot-points.

The minima in the polar cap and auroral oval are less than 10 cm^{-3} under winter conditions. The lowest values (< 0.1 cm^{-3}) are in the pre-midnight sector of the auroral zone. Under summer (illuminated) conditions, the minimum density values range from $\sim$ 1 - 20 cm^{-3} with values frequently over 10 cm^{-3} except around noon in the auroral zone where minimum values are from $\sim$ 1 - 10 cm^{-3}. Upon sorting by foot-point illumination, the minimum values in the seasonal summer plot on the night-side of Plate 3c are removed providing evidence that the low density measurements are correlated with the absence of ionospheric illumination.

The altitude variation for the data set in the noon-midnight and dawn-dusk meridians is shown in Plate 4. Data are averaged in MLT for 6 hours centered on the noon-midnight and the dawn-dusk meridian for illuminated and non-illuminated ionospheric conditions. The data ranges from 1.8 to 2.4 Re geocentric radial distance under illuminated and non-illuminated ionospheric conditions. Radial distances of 2 Re and 3 Re geocentric and magnetic field lines corresponding to invariant latitudes 80, 70, 60 and 50 degrees are shown.

4. Summary and Discussion

Using the spacecraft potential measurements from the Polar EFI for one year of perigee passes from April 15, 1996 to April 15, 1997, we have made the first synoptic maps of the thermal plasma density in the auroral zone and polar cap at an altitude of $\sim$1 Re, at all local times. The maps show that there is a large scale density cavity in the auroral zone which extends to all local times except noon. The depth of this cavity and the density in the polar cap both depend very strongly on the solar illumination of the ionosphere. The average plasma density for illuminated (summer) conditions is a factor of $\sim$5 larger than for non-illuminated (winter) conditions.

The average density in the auroral zone under non-illuminated conditions is $\sim$5-10 cm^{-3}; whereas under illuminated conditions, it is $\sim$20-40 cm^{-3}. During winter, the lowest average plasma density is $\sim$few tenths cm^{-3} at $\sim$19 MLT and $\sim$72 degrees ILAT. The density is depleted below the average cavity density near $\sim$15-24 MLT and $\sim$3-5 MLT. Higher values of the standard deviation in the region of the large scale density cavity indicate large fluctuations of plasma density. Possible reasons for this are variations in small scale structures, the overall cavity depth, or the location of the polar cap boundary. Movement of the polar cap boundary appears to be a smaller effect because the increased standard deviation would be visible in both the illuminated and non-illuminated cases. The maps presented herein confirm the results of *Calvert* [1981] and *Persoon et al.* [1988], who provided statistical information on the altitude dependence of the cavity over a limited local time and latitude range.

In the polar cap, the average density in darkness is $\sim$20 cm^{-3}; in sunlight, it is $\sim$100 cm^{-3}. When the entire polar cap is illuminated, there is a region of strong density enhancement in the polar cap except for 20 - 4 MLT on the night-side. This region disappears when the polar cap is in darkness. The density enhancement in the polar cap could be due to an increased ionospheric scale height due to higher temperature. There is also a slight increase in standard deviation of the polar cap under non-illuminated conditions. These observations provide direct evidence for the control of solar illumination on the polar wind density at altitudes of $\sim$ 1 Re.

The density structure in the high latitude ionosphere is controlled by the complex interplay between the time and spatial variation of the ionization created by solar illumination and plasma transport processes operating parallel and perpendicular to the geomagnetic field. The maps described above show that, at altitudes of 1 Re, the transport processes together create a cavity at auroral latitudes at all local times, except noon, whether or not these regions are in sunlight or darkness. The transport mechanisms which result in outflow parallel to the magnetic field include acceleration by parallel electric fields, perpendicular heating in combination with the magnetic mirror force, and, on the polar cap field lines, the supersonic expansion of the polar wind. Perpendicular transport is primarily due to the **ExB** convection of the plasma in both large-scale and small-scale electric fields.

A possible mechanism for the generation of density cavities in the region of upward field-aligned currents is due to the trapping of low energy ionospheric electrons. In the region of upward field-aligned currents, parallel electric fields (which energize plasma sheet electrons to produce the aurora) accelerate ion beams out of the ionosphere and also reflect low energy electrons, trapping them between the potential structure and their low altitude mirror points. FAST measurements have shown that the dominant contribution to the electron density in the density cavities associated with ion beams are energetic plasma sheet electrons [*Strangeway et al.*, 1998; *McFadden et al.*, 1999]. Outside these regions, measurements from the S3-3 Langmuir probe [*Kletzing et al.*, 1998] show that the electron density is primarily due to electrons with energies of a fraction of an eV (ionospheric electrons).

Another candidate mechanism for creating auroral density cavities is the acceleration of ion conic distributions. Ion conics are generated through strong heating of ions perpendicular to the magnetic field by intense wave fields [*Liu et al.*, 1994; *Shelley*, 1995; *Carlson et al.*, 1998]. The effect of the magnetic mirror force associated with the diverging magnetic field geometry, converts perpendicular to parallel energy, and accelerates the ions away from the earth. The electron density is depleted in a manner consistent with quasi-neutrality. The reduction of the density in the cavity alters the index of refraction of auroral field lines for the propagation of a variety wave modes including those that are likely to generate the parallel and perpendicular electric fields which create the density depletion. An example of such an interaction is demonstrated in a simulation by *Ganguli et al.* [1988] showing the generation of density cavities through feedback between field-aligned currents and the onset of of electrostatic ion cyclotron waves. The fine-scale structure of field-aligned currents is likely to be strongly influenced by the structure of plasma density depletion since such depletions alter the charge carriers necessary to carry the current. Thus, there are likely to be a variety of non-linear mechanisms involving feedback between the electric fields that accelerate plasma, the creation of the density depletion and the modification of the structure of the electric fields as they interact with the density cavity.

Comparison of the density structure illustrated in the maps presented herein and previous statistical studies of auroral phenomena may aid in determining which transport mechanisms and illumination effects are most important. For both illuminated and non-illuminated conditions, the region of density depletion agrees with the average location of indicators of auroral acceleration such as electrostatic shocks, accelerated electron distributions, ion beams and field-aligned currents. *Newell et al.* [1996a] examined the probability of observing accelerated electron distributions without regard to season. They showed that the maximum probability for events greater than 0.25 erg/cm^{2}s occurred from 18-24 MLT near 70 degrees and near 15 MLT at ~72 degrees. These are the same locations where deep density depletions can be seen in Plates 1a and 1b, which suggests that parallel electric fields in the upward current region may be associated with the density cavity in this region. The probability of observing accelerated electrons in the morning-side (~3-9 MLT) is lower, although the density cavity is still seen.

There have also been several previous statistical studies which have specifically addressed the issue of seasonal dependence. Because it also used data from Polar perigee passes obtained from October, 1996 through September, 1997 (compared to April, 1996 through April, 1997 for our study), the study of *Collin et al.* [1998] on the seasonal variation in up-flowing ion beams can be most directly compared to our thermal density maps. Their Figure 1 (winter conditions) shows that the magnetic local time and invariant latitude dependence of the regions of high occurrence probability of up-flowing ion beams is very similar to that of the regions of lowest density in the auroral zone for winter conditions. The only difference is that they do not see an enhanced probability of up-flowing ions in the 3-6 MLT sector. Similarly, their Figure 2 (summer), which showed that the probability decreased by a factor of 2-3, had an ILAT-MLT dependence which is almost identical to our Plates 1b and 1d. Because ion beams are

indicative of a parallel potential below the spacecraft, the agreement between the location of density depletions and ion beams is consistent both with mechanisms for parallel electric fields which require reduced density and with the creation of the cavity by parallel electric fields. They found no seasonal dependence in the occurrence of ion conics (which have their largest occurrence frequency between ~9 and 12 MLT).

Newell et al. [1996b] produced maps of the occurrence probability of intense aurora (defined as having energy flux > 5 ergs/cm^{2}s) for sunlit and dark conditions, using electron distribution function data from the DMSP satellites. They found that intense events, which were primarily restricted to the dusk sector (~19-23 MLT) at invariant latitudes of ~68-72 degrees, were a factor of ~3 more probable in dark compared to sunlit conditions. Intense aurora were also observed, but with a much smaller occurrence probability and latitudinal extent, near 15 MLT and in the morning. The results presented herein indicate that the density depletion in the auroral zone is also ~2-5 times less in sunlight than in darkness.

Bennett et al. [1983] showed data consistent with a decreased occurrence frequency of electrostatic shocks in the summer compared to winter. Since electrostatic shocks have been shown to be correlated with parallel electric field auroral acceleration [*Mozer et al.*, 1980; *McFadden et al.*, 1999], this is consistent with the studies of *Newell et al.* [1996b] and *Collin et al.* [1998]. The S3-3 study was limited by the seasonally-locked nature of the spacecraft orbit, however, so detailed local time and invariant latitude dependence could not be determined.The seasonal dependence of the average strength of auroral emissions described by *Liou et al.* [1997] is also consistent with the above referenced studies.

Carlson et al. [1998] report seasonal variations of electron beams in downward field-aligned current regions and ion beams in neighboring upward field-aligned regions. They argue that these observations are consistent with the role played by ion scale height in the generation of electrostatic structures responsible for particle acceleration. *Laakso et al.* [2000], using the same data set presented here, show a seasonal variation in the plasma density integrated over the entire polar cap above 82 degrees. Our study indicates that this average seasonal variation may be due to the percentage of time the polar cap is illuminated as the orientation of the magnetic dipole changes with respect to the sun throughout the year.

Seasonal variations have also been observed in the production of auroral kilometric radiation. *Kasaba et al.* [1997] show AKR is more active in the winter hemisphere for higher frequency ranges (500 kHz). *Kumamoto and Oya* [1998], in a study restricted to the 18-24 MLT sector, showed a seasonal dependence of auroral kilometric radiation (AKR) with emissions in the winter hemisphere being more intense and more common. They concluded that their finding were consistent with the *Newell et al.* [1996a] results on intense electron beams. In addition, they showed that the seasonal dependence was stronger for the higher frequency emissions. This is very consistent with our observations of the seasonal dependence of the densities within the cavity. AKR is produced at the electron cyclotron frequency so that higher frequencies are emitted at lower altitudes. Since $\omega_{pe}/\omega_{ce} < 1.0$ is a necessary condition for the generation of auroral kilometric radiation by the relativistic Doppler shifted cyclotron maser instability, AKR is more likely to be generated at higher frequencies in the winter when the cavity densities are lower.

Most studies of the seasonal dependence of auroral phenomena have attributed the observed variations to the difference in the ionospheric conductivity obtained for sunlit versus dark conditions (see, for example, *Newell et al.* [1996b]). Our experimental results suggest that another important factor maybe the difference in the thermal plasma density. One often invoked class of auroral acceleration mechanisms postulates that parallel electric fields are established when the field-aligned current density exceeds the current carrying capacity of the plasma which depends on density and thermal velocity. Such mechanisms would result in parallel electric fields occurring most frequently in low density regions under non-illuminated conditions. Ongoing studies of field-aligned currents and large electric fields will aid in determining the relative importance of conductance and density in controlling auroral acceleration. The study described herein also points out the importance of microscopic processes in determining meso-scale structures.

Acknowledgments. This research was supported by NASA Grant NAG5-3182.

References

Bennett, E. L., M. Temerin, and F. S. Mozer, The distribution of auroral electrostatic shocks below 8000-km altitude, *J. Geophys. Res., 88,* 7107, 1983.

Block, L. P. and C.-G. Fälthammar, Characteristics of magnetic field aligned electric fields in the auroral acceleration

region, in *Auroral Physics*, edited by Meng, Rycroft, and Frank, Cambridge University Press, 1991.

Boström, R., G. Gustafsson, B. Holback, G. Holmgren, H. Koskinen, and P. Kintner, Characteristics of solitary waves and weak double layers in the magnetospheric plasma, *Phys. Rev. Lett., 61,* 82, 1988.

Calvert, W., The auroral plasma cavity, *Geophys. Res. Lett., 8,* 8, 919, 1981.

Carlson, C. W., J. P. McFadden, R. E. Ergun, M. Temerin, W. Peria, F. S. Mozer, D. M. Klumpar, E. G. Shelly, W. K. Peterson, E. Moebius, R. Elphic, R. Strangeway, C. Cattell, and R. Pfaff, FAST observations in the downward auroral current region: Energetic upgoing electron beams, parallel potential drops, and ion heating, *Geophys. Res. Lett., 25,* 12, 2017, 1998.

Collin, H. L., W. K. Peterson, O. W. Lennartsson, and J. F. Drake, The seasonal variation of aurora ion beams, *Geophys. Res. Lett., 25,* 4071, 1998.

Ergun, R. E., C. W. Carlson, J. P. McFadden, F. S. Mozer, G. T. Delory, W. Peria, C. C. Chaston, M. Temerin, I. Roth, L. Muschietti, R. Elphic, R. Strangeway, R. Pfaff, C. A. Cattell, D. Klumpar, E. Shelley, W. Peterson, E. Moebius, and L. Kistler, FAST observations of large-amplitude solitary structures, *Geophys. Res. Lett., 25,* 2041, 1998.

Escoubet, C. P., A. Pedersen, R. Schmidt, and P. A. Lindqvist, Density in the magnetosphere inferred from ISEE 1 spacecraft potential, *J. Geophys. Res., 102,* 17595, 1997.

Ganguli, Supriya B., Peter J. Palmadesso, and Horance G. Mitchell, Effects of electron heating on the current driven electrostatic ion cyclotron instability and plasma transport processes along auroral field lines, *Geophys. Res. Lett., 15,* 11, 1291, 1988.

Grard, Réjean J. L., Properties of the satellite photoelectron sheath derived from the photoemission laboratory measurements, *J. Geophys. Res., 78,* 2885, 1973.

Harvey, P., F. S. Mozer, D. Pankow, J. Wygant, N. C. Maynard, H. Singer, W. Sullivan, P. B. Anderson, R. Pfaff, T. Aggson, A. Pedersen, C.-G. Fälthammar, and P. Tanskannen, The electric field instrument on the POLAR satellite, *Space Sci. Rev., 71,* 583, 1995.

Kasaba, Y., H. Matsumoto, K. Hashimoto, and R. R. Anderson, The angular distribution of auroral kilometric radiation observed by the GEOTAIL spacecraft, *Geophys. Res. Lett., 24,* 2483, 1997.

Kletzing, C. A., F. S. Mozer, and R. B. Torbert, Electron temperature and density at high latitude, *J. Geophys. Res., 103,* 14837, 1998.

Kumamoto, Atsushi and Hiroshi Oya, Asymmetry of occurrence-frequency and intensity of AKR between summer polar region and winter polar region sources, *Geophys. Res. Lett., 25,* 2369, 1998.

Laakso, H., R. Pfaff, et al., Polar observations of electron density distribution in the earth's magnetosphere, *J. Geophys. Res.,* 2000.

Laakso, H., N. C. Maynard, R. F. Pfaff, T. L. Aggson, W. R. Coley, P. Janhunen, and F. A. Herrero, Electric field diagnostics of the dynamics of equatorial density depletions, *J. Atmos. Sol.-Terr. Phys., 59,* 1625, 1997.

Liou, K., P. T. Newell, C.-I. Meng, M. Brittnacher, and G. Parks, Synoptic auroral distribution: A survey using Polar ultraviolet imagery, *J. Geophys. Res., 102,* 27197, 1997.

Liu, Chau, J. D. Perez, T. E. Moore, C. R. Chappell, and J. A. Slavin, Fine structure of low-energy H+ in the nightside auroral region, *J. Geophys. Res., 99,* 4131, 1994.

McFadden J. P., C. W. Carlson, and R. E. Ergun, Microstructure of the auroral acceleration region as observed by FAST, *J. Geophys. Res., 104,* 14453, 1999.

Mott-Smith, H. M., and Irving Langmuir, The theory of collectors in gaseous discharges, *Phys. Rev., 28,* 727, 1926.

Mozer, F. S., C. W. Carlson, M. K. Hudson, R. B. Torbert, B. Parady, J. Yatteau, and M. C. Kelley, Observations of paired electrostatic shocks in the polar magnetosphere, *Phys. Rev. Lett., 38,* 292, 1977.

Mozer, F. S., C. A. Cattell, M. Temerin, R. B. Torbert, S. Von Glinski, M. Woldorff, and J. Wygant, The DC and AC electric field, plasma density, plasma temperature, and field-aligned current experiments on the S3-3 satellite, *J. Geophys. Res., A10,* 5875, 1979.

Mozer, F. S., C. A. Cattell, R. L. Lysak, M. K. Hudson, M. Temerin, Satellite measurements and theories of low altitude auroral particle acceleration, *Space Sci. Rev., 27,* 155, 1980.

Mozer, F. S., R. Ergun, M. Temerin, C. Cattell, J. Dombeck, J. Wygant, New features of time domain electric-field structures in the auroral acceleration region, *Phys. Rev. Lett., 79,* 1281, 1997.

Nakagawa, Tomoko, Takuma Ishii, Koichiro Tsundra, Hajime Hayakawa, and Toshifumi Mukai, Net current density of photo electrons emitted from the surface of the Geotail spacecraft, *Earth Planets Space, 52,* 283, 2000.

Newell, Patrick T., Kevin M. Lyons, and Ching-I. Meng, A large survey of electron acceleration events, *J. Geophys. Res., 101,* 2599, 1996a.

Newell, Patrick T., Ching-I. Meng, and Kevin M. Lyons, Suppression of discrete aurorae by sunlight, *Nature, 381,* 766, 1996b.

Pedersen, A., Solar wind and magnetosphere plasma diagnostics by spacecraft electrostatic potential measurements, *Ann. Geophysicae, 13,* 118, 1995.

Persoon, A. M., D. A. Gurnett, W. K. Peterson, J. H. Waite, Jr., J. L. Burch, and J. L. Green, Electron density depletions in the nightside auroral zone, *J. Geophys. Res., 93,* 1871, 1988.

Schott, L., Chapter 11: Electrical probes, in *American Vacuum Society Classics: Plasma Diagnostics*, edited by W. Lochte-Holtgreven, pp. 668-731, American Institute of Physics, New York, 1995.

Scudder J., F. Hunsacker, G. Miller, J. Lobell, T. Zawistowski, K. Ogilvie, J. Keller, D. Chornay, F. Herrero, R. Fitzenreiter, D. Fairfield, J. Needell, D. Bodet, J. Googins, C. Kletzing, R. Torbert, J. Vandiver, R. Bentley, W. Fillius, C. McIlwain, E. Whipple, and A. Korth, Hydra -

A 3-dimensional electron and ion hot plasma instrument for the Polar spacecraft of the GGS mission, *Space Sci. Rev., 71,* 459, 1995.

Scudder, J. D., Xuejun Cao, and F. S. Mozer, Photoemission current-spacecraft voltage relation: key to routine, quantitative low-energy plasma measurements, *J. Geophys. Res., 105,* 21281, 2000.

Shelley, E. G., The auroral acceleration region: The world of beams, conics, cavitions, and other plasma exotica, *Rev. Geophys., Supplement, 709,* 1995.

Strangeway R. J., L. Kepko, R. C. Elphic, C. W. Carlson, R. E. Ergun, J. P. McFadden, W. J. Peria, G. T. Delory, C. C. Chaston, M. Temerin, C. A. Cattell, E. Möbius, L. M. Kistler, D. M. Klumpar, W. K. Peterson, E. G. Shelley, and R. F. Pfaff, FAST observations of VLF waves in the auroral zone: Evidence of very low plasma densities, *Geophys. Res. Lett., 25,* 2065, 1998.

Temerin, M., C. A. Cattell, R. Lysak, M. Hudson, R. B. Torbert, F. S. Mozer, R. D. Sharp, and P. M. Kitner, The small scale structure of electrostatic shocks, *J. Geophys. Res., 86,* 11278, 1984?.

M. T. Johnson, J. R. Wygant, and C. Cattell, School of Physics and Astronomy, 116 Church Street SE, Minneapolis, MN 55455.

F. S. Mozer and M. Temerin, Space Science Laboratory, University of California, Berkeley, CA, 94720.

J. Scudder, Department of Physics and Astronomy, University of Iowa, Iowa City, IA, 52242.

Received May 8, 1996; revised August 10, 1996; accepted October 12, 2000.

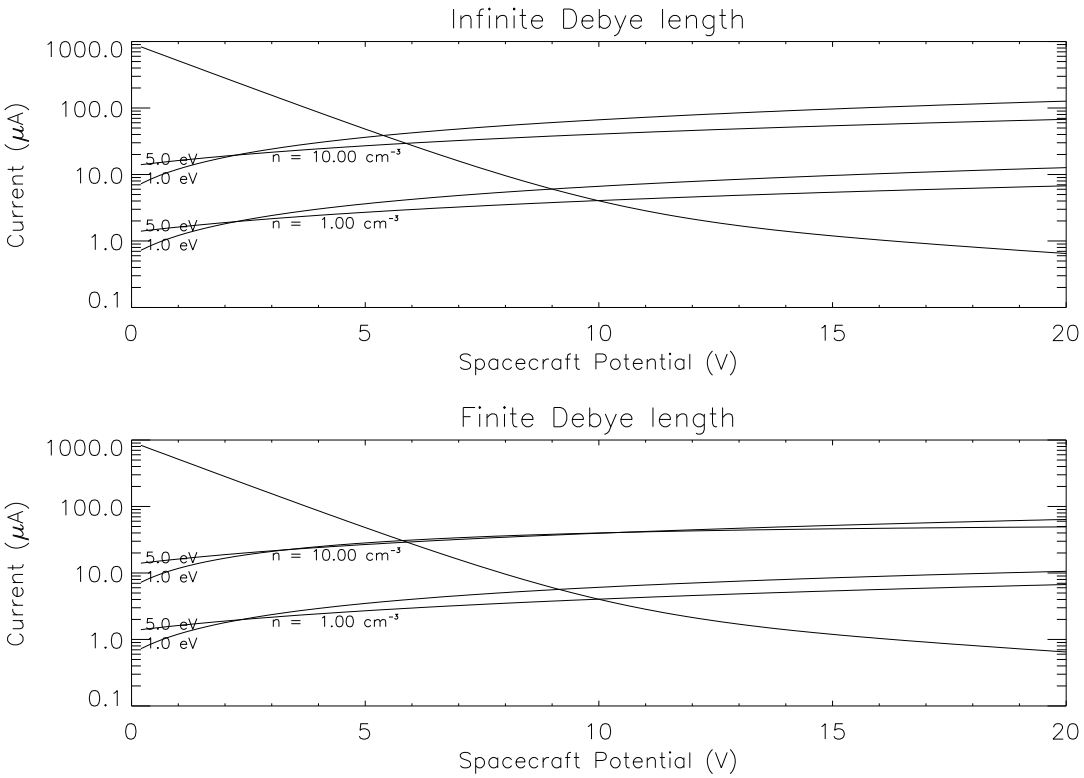

Figure 1. Photoelectric and thermal currents as a function of spacecraft potential for plasmas with electron densities of 1.0 and 10.0 cm^{-3} with temperatures of 1.0 and 5.0 eV. The upper and lower plots show cases for infinite and finite sheath lengths, respectively.

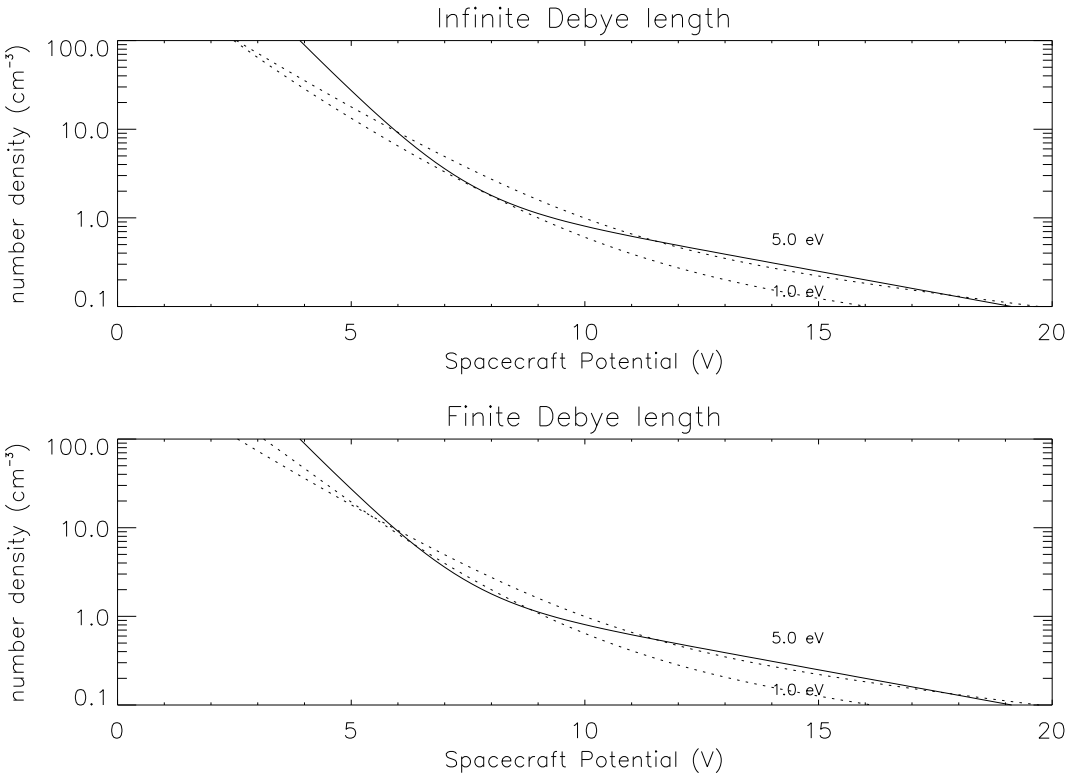

Figure 2. Theoretical calculation of electron number density as a function of spacecraft potential using $A = 22.6m^{-2}$ and $A_\nu = 6.16m^{-2}$. The dashed lines are the calculated number density using plasma temperatures 1.0 and 5.0 eV. The solid line is the calibration provided in equation (5).

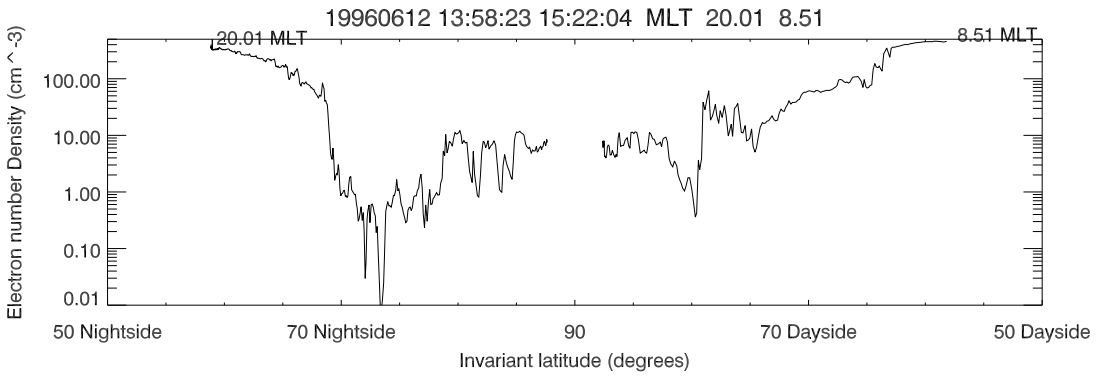

Figure 3. A southern hemisphere pass for June 12, 1996 showing the thermal plasma density before averaging.

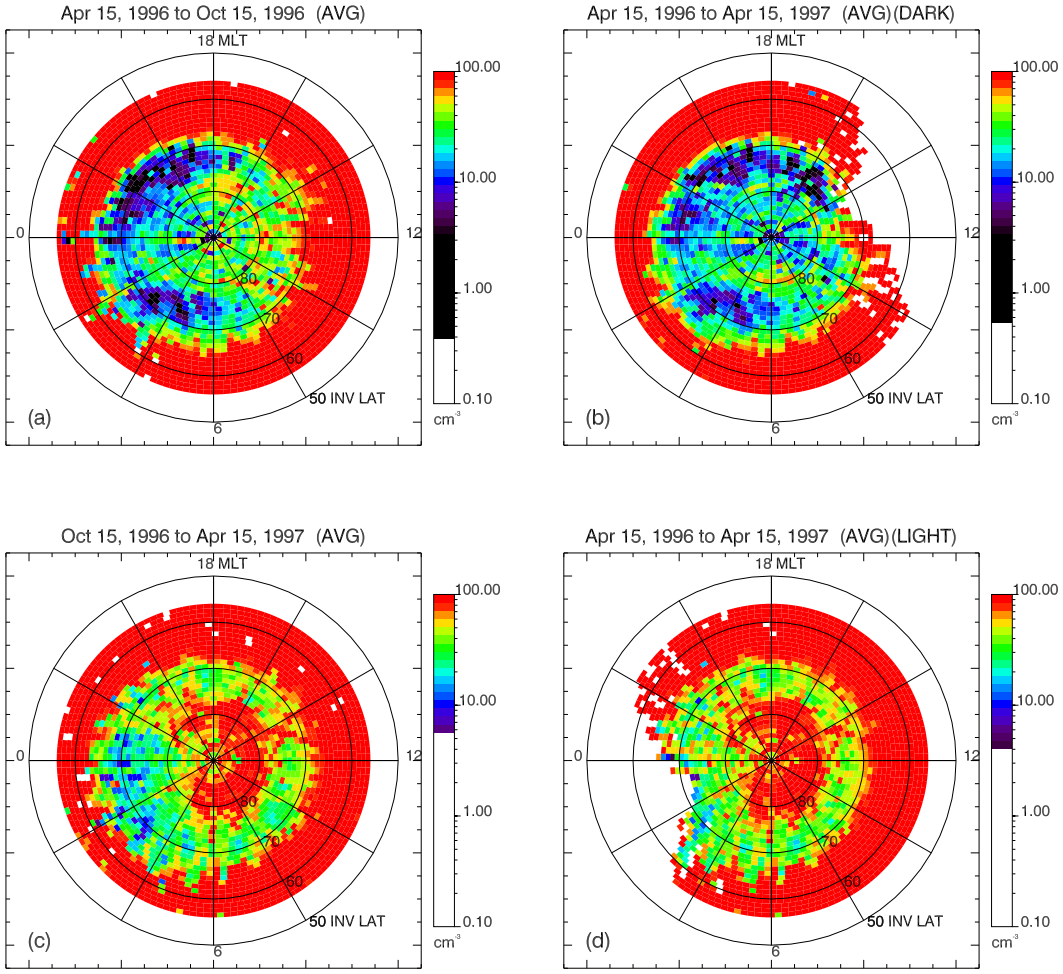

Plate 1. Synoptic maps of the southern hemisphere using data for a year starting April 15, 1996. The figures show (a) the winter months from April 15, 1996 to October 15, 1996, (b) the entire year selecting data for dark ionospheric conditions, (c) the summer months from October 15, 1996 to April 15, 1997, and (d) the entire year selecting data for sunlit ionospheric conditions.

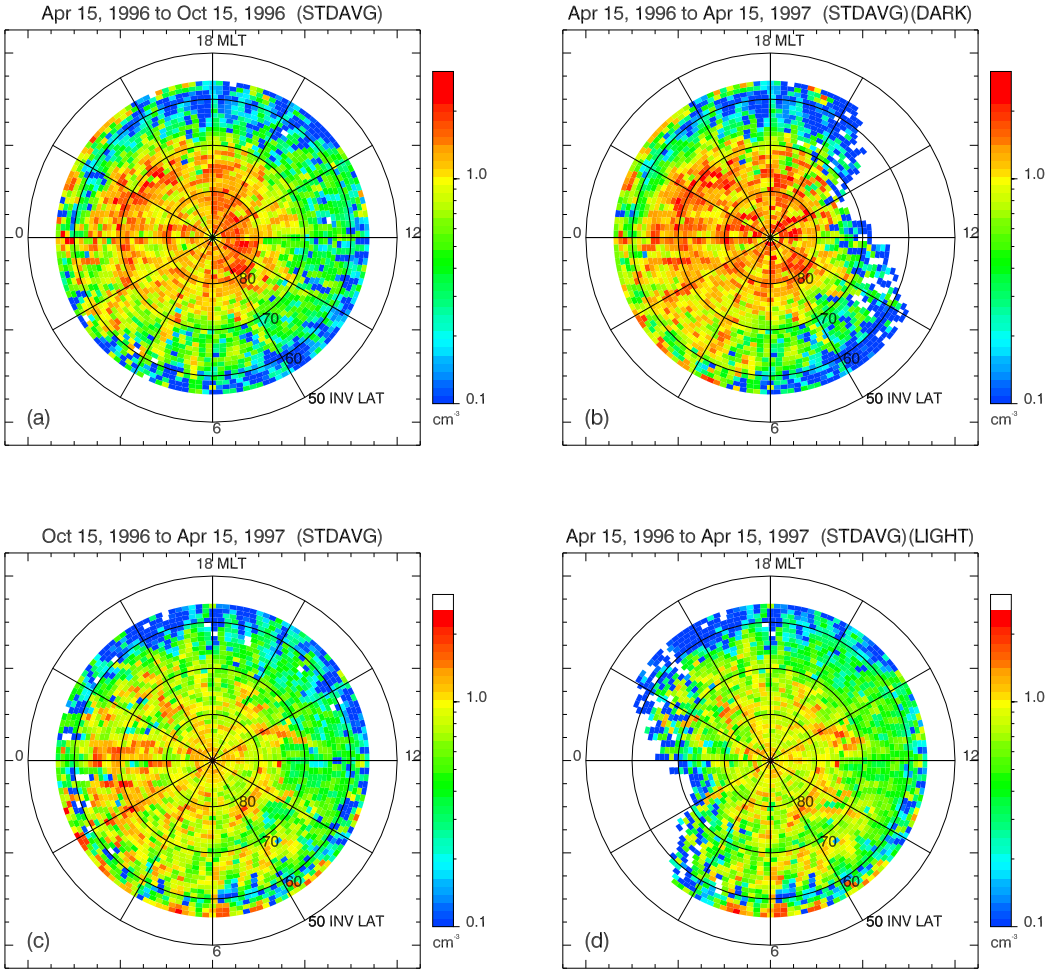

Plate 2. The standard deviation the data bins shown in Plate 1. The figures show standard deviation for (a) the winter months from April 15, 1996 to October 15, 1996, (b) the entire year selecting data for dark ionospheric conditions, (c) the summer months from October 15, 1996 to April 15, 1997, and (d) the entire year selecting data for sunlit ionospheric conditions.

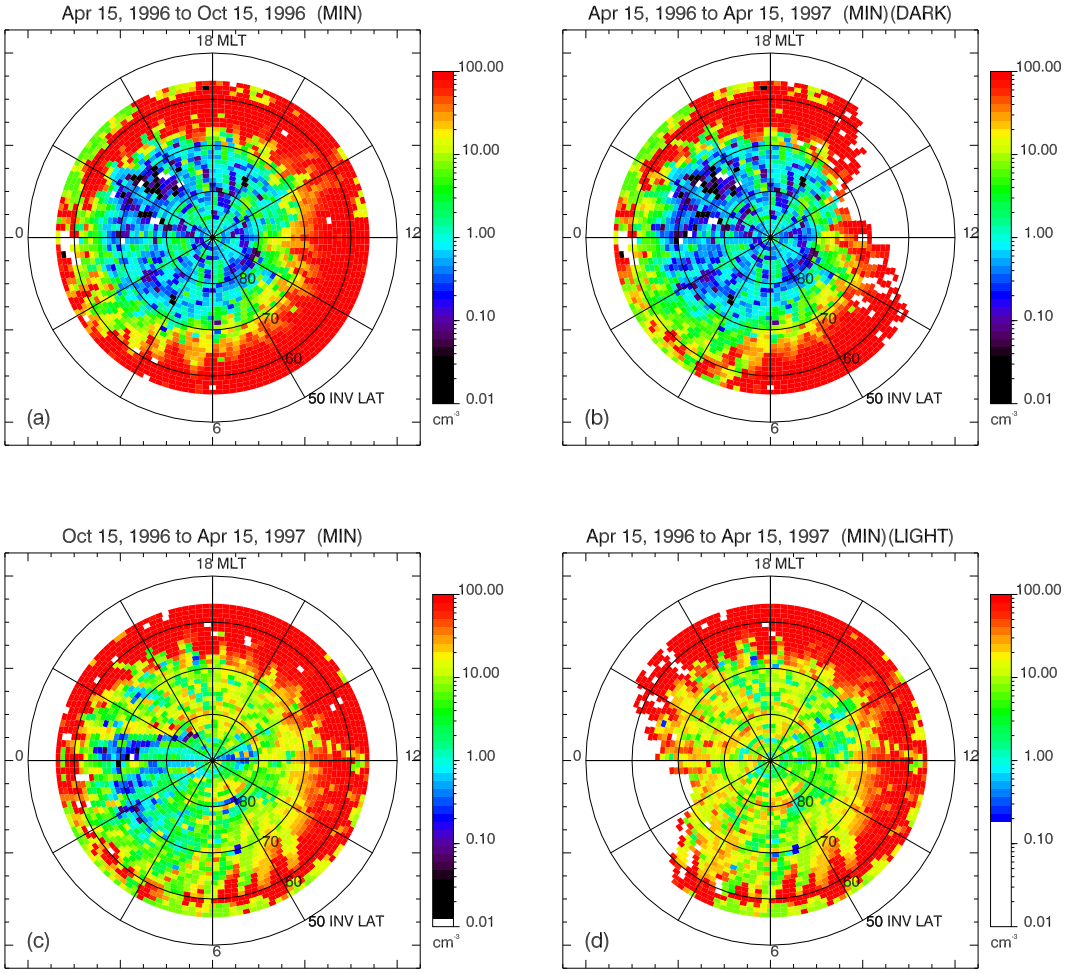

Plate 3. The minimum values for the data bins shown in Plate 1. The figures show minimum values for (a) the winter months from April 15, 1996 to October 15, 1996, (b) the entire year selecting data for dark ionospheric conditions, (c) the summer months from October 15, 1996 to April 15, 1997, and (d) the entire year selecting data for sunlit ionospheric conditions.

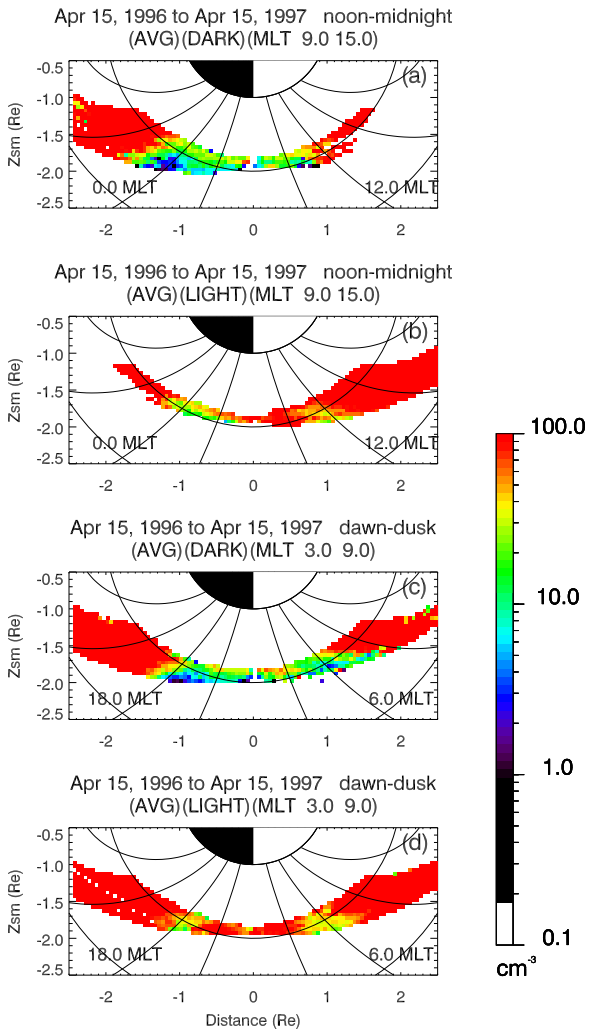

Plate 4. The density profiles for the entire year of data under non-illuminated and illuminated conditions for (a,b) the noon-midnight and (c,d) the dawn-dusk meridians.